

Bacterial infection-mediated mucosal signalling induces local renal ischaemia as a defence against sepsis

Keira Melican,^{1,2} Jorrit Boekel,^{1,2} Lisa E. Månsson,^{2†} Ruben M. Sandoval,³ George A. Tanner,⁴ Örjan Källskog,⁵ Fredrik Palm,^{5,6} Bruce A. Molitoris³ and Agneta Richter-Dahlfors^{1,2*}

Departments of ¹Neuroscience and ²Microbiology, Tumor and Cell Biology, Karolinska Institutet, Stockholm, S-171 77, Sweden.

³Division of Nephrology, Department of Medicine, Indiana Center for Biological Microscopy, Indianapolis, IN 46202, USA.

⁴Department of Cellular and Integrative Physiology, Indiana University School of Medicine, Indianapolis, IN 46202, USA.

⁵Department of Medical Cell Biology, Uppsala University, Uppsala, S- 751 23, Sweden.

⁶Department of Medicine, Division of Nephrology and Hypertension, Georgetown University, Washington, DC 20007, USA.

Summary

Ascending urinary tract infections can cause extensive damage to kidney structure and function. We have used a number of advanced techniques including multiphoton microscopy to investigate the crucial early phases of uropathogenic *Escherichia coli* induced pyelonephritis within a living animal. Our results reveal a previously undescribed innate vascular response to mucosal infection, allowing isolation and eradication of the pathogen. The extremely rapid host response to mucosal infection was highlighted by the triggering of a cascade of events within 3–4 h. Epithelial signalling produced an increase in cellular O₂ consumption and affected microvascular flow by clotting, causing localized ischaemia. Subsequent ischaemic damage affected pathophysiology with actin re-arrangement and epithelial sloughing leading to paracellular bacterial movement. A denuded tubular basement membrane is shown to hinder

immediate dissemination of bacteria, giving the host time to isolate the infection by clotting. Suppression of clotting by heparin treatment caused fatal urosepsis. Clinically these findings may be relevant in antibiotics delivery in pyelonephritis patients and to the use of anticoagulants in sepsis.

Introduction

Pyelonephritis, a bacterial infection of the kidneys, is commonly caused by uropathogenic *Escherichia coli* (UPEC) ascending from the lower urinary tract into the renal tubular system (Hill, 1989). This condition has been linked to a number of debilitating disorders such as renal failure, hypertension and end-stage kidney disease (Jahnukainen *et al.*, 2005). The histological hallmarks of acute pyelonephritis include the formation of abscesses, oedema and scarring (Ronald and Nicolle, 2002). The accumulation of polymorphonuclear leucocytes (PMNs) in the infected area has been observed and linked to extensive tissue damage (Hill, 1989; Ronald and Nicolle, 2002; Schaeffer, 2002). The exact order of events leading to such dramatic alteration of tissue homeostasis, as well as its molecular basis, is however, currently unknown.

We recently described the real-time progression of infection within the living kidney using multiphoton microscopy (Månsson *et al.*, 2007). This work revealed a very short time frame (< 22 h), from initial contact of bacteria with the epithelial proximal tubule lining to the characteristic tissue damage associated with acute pyelonephritis and bacterial clearance. Dramatic effects on local peritubular capillaries were observed early during the infection process, while bacteria were still maintained within the lumen of the proximal tubule (Månsson *et al.*, 2007).

Any disruption of renal flow is of vital importance with the highly vascularized kidneys receiving 20% of the total cardiac output (O'Callaghan, 2006). Renal ischaemic injury, resulting from a reduction, or absence, of blood supply, has been shown to dramatically influence the renal tissue homeostasis, with ATP depletion affecting transport (Goldfarb *et al.*, 2002), cellular morphology (Ashworth *et al.*, 2001) and tubular integrity (Goligorsky and DiBona, 1993, Molitoris and Marrs, 1999). A majority

Received 25 March, 2008; revised 14 May, 2008; accepted 23 May, 2008. *For correspondence. E-mail agneta.richter.dahlfors@ki.se; Tel. (+46) 8 52487425; Fax (+46) 8 333864. †Present address: Division of Gastroenterology, BC Children's Hospital, University of British Columbia, Vancouver, British Columbia V5Z 4H4, Canada.

of reports studying the effects of infection on renal blood flow, have used either haematogenous or septic models, such as cecal ligation and puncture (Ivanyi, 1991; Langenberg *et al.*, 2005). The infectious agent thus enters the bloodstream immediately where it elicits a systemic response as well as interacting directly with the endothelium. Areas of ischaemic damage have been observed and are suggested to be caused by occlusion of peritubular capillaries by adherent PMNs and vasoconstriction, but little molecular detail is known (Ivanyi, 1991; Ronald and Nicolle, 2002; Jahnukainen *et al.*, 2005). In ascending urinary tract infection (UTI), bacteria are localized within the lumen of proximal tubules rather than the vasculature. As a result, previously reported haematogenous data may hold little relevance when studying ascending infections.

Extensive investigation has been performed on the innate host defences to mucosal bacterial infection (Sansonetti, 2006). Within the kidney, urine flow (Schaeffer, 2001), antimicrobial peptides (Chromek *et al.*, 2006), hormones such as vasopressin (Chassin *et al.*, 2007) and the Toll-like receptor 4 signalling pathway (Backhed *et al.*, 2001; Svanborg *et al.*, 2001; El-Achkar *et al.*, 2006) are all factors in this immunity. As the ascending UTI model suffers from poor temporal control, it is likely however, that other mechanisms, operating within the first few hours of infection, also exist.

The development of a real-time kidney infection model, where bacteria are seeded intraluminally, by microperfusion, helps overcome the lack of spatial-temporal control inherent in other ascending pyelonephritis models (Mansson *et al.*, 2007). Multiphoton microscopy allows for observation of the earliest stages of infection, when prevention of tissue damage is most crucial (Smellie *et al.*, 1994). The living model also allows for the observation of physiological factors such as blood flow which are lacking in other models. The present study focuses on the molecular mechanisms, and consequences, of infection-mediated alterations on renal tissue homeostasis. Our results highlight the rapidity, localization and multifactorial basis behind the host response to infection. We describe how mucosal infection triggers epithelial signalling resulting in a rapid, indirect, vascular response which functions to isolate the invading pathogen.

Results

Infection-mediated peritubular capillary disturbances occur independently of glomerular changes

To analyse the effects bacterial infection exerts on renal vasculature, the lumen of single nephrons of exposed rat kidneys was microperfused with GFP⁺-expressing LT004, a variant of the prototypic UPEC strain CFT073, or an

equivalent PBS solution. The progression of infection was observed using multiphoton fluorescence microscopy (Mansson *et al.*, 2007). S1 segments of proximal tubules in close proximity to superficial glomeruli were chosen for infusion to allow for simultaneous observation of both peritubular and glomerular capillaries (Fig. 1A). Infused bacteria were subjected to tubular fluid flow, and bacteria adhering to the mucosa were initially scarce. As bacteria began to multiply and fill the tubule lumen, blood flow in surrounding peritubular capillaries declined and stopped, as early as 3 h post infusion. The stoppage was noted by the lack of blood plasma marker and reduced capillary diameter. Reductions around 20 µm were commonly observed. Adjacent glomeruli appeared relatively unaffected. Only occasional glomerular capillary loops showed signs of congestion as late as 8.5 h post infusion. PBS-infused control S1 sites within the same kidney demonstrated no changes in peritubular or glomerular capillaries (Fig. 1B).

A line scan method (Kleinfeld *et al.*, 1998) was employed to obtain quantification of blood flow rates within peritubular capillaries of infected and uninfected nephrons (Fig. S1). A peritubular capillary, horizontal to the field of view, was scanned along its central axis at 2 ms per line for 4 s. Individual red blood cell (RBC) velocity was determined by the distance it had travelled through the vessel over a defined time period. These measurements demonstrated a rapid, highly localized, decline of blood flow rates upon bacterial colonization of the proximal tubule epithelia (Fig. 1C). Control PBS-infused sites showed no decrease in blood flow rates (Fig. 1D). Due to variability in vessel size and location, comparisons between the two sites are not feasible. Vessel analysis from Fig. 1 is shown in Fig. S1.

Infection causes an immediate drop in local tissue oxygen tension

The decline in blood flow suggested that the infection process may cause an alteration in oxygen availability in the tissue. Clark-type microelectrodes were used to continuously measure tissue oxygen tension (PO₂), within the lumens of infused tubules. The recordings were initiated immediately following bacterial infusion, when bacterial numbers were low. A significant drop ($P < 0.001$) was observed as early as 1 h post infusion, and within 3.5–4 h the PO₂ dropped to 0 mmHg (Fig. 2A). Measurements were simultaneously taken within PBS-infused sham nephrons of the same kidney, with PO₂ levels remaining stable around 48 mmHg, corresponding to readings from untouched cortex (Fig. 2A). To rule out any systemic involvement in the infection-associated drop in PO₂, arterial blood pressure was monitored throughout the experiment (Fig. 2B). Spatial mapping of the area surrounding

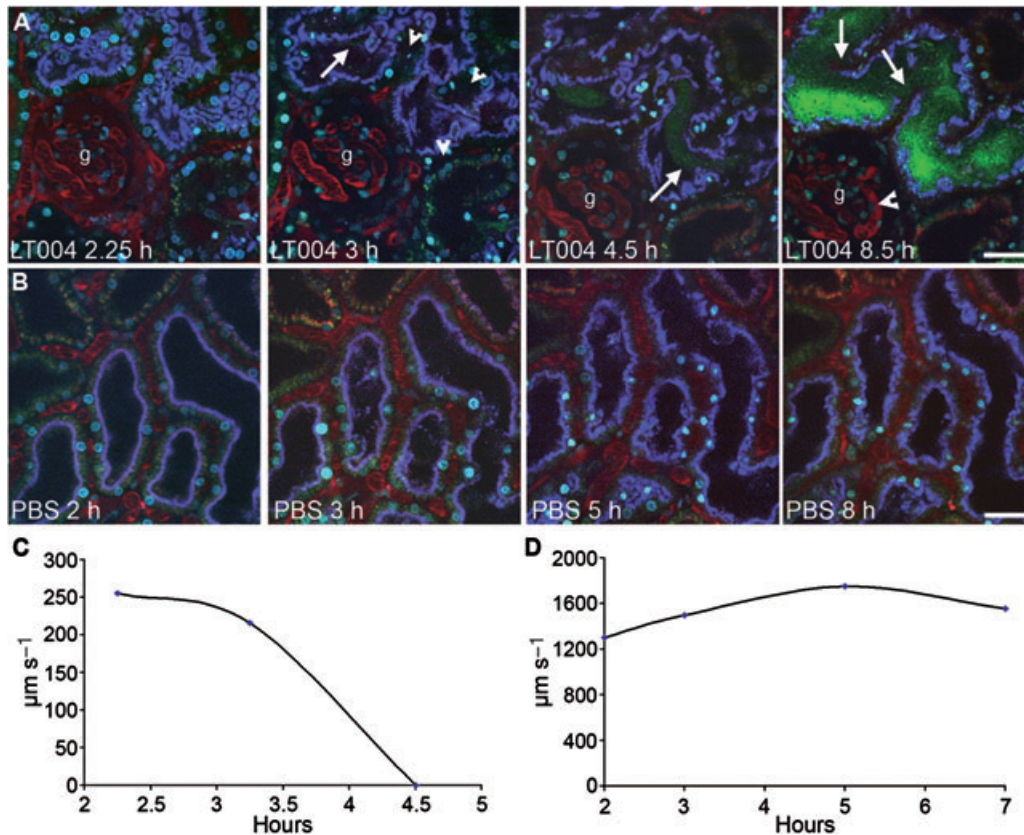


Fig. 1. Infection-mediated vasculature dysfunction.

A. Representative real-time visualization of tissue responses in an infected proximal tubule (outlined by endocytosed blue dextran), by multiphoton microscopy. At 2.25 h, normal blood flow, labelled with a large molecular weight fluorescently labelled dextran (red), was seen in peritubular and glomerulus (g) capillaries. RBCs are seen as black streaks within vessels. At 3 h, a few bacteria (green) adhered to the tubule lining (arrow), and peritubular capillaries showed signs of collapse and altered flow (arrowheads). At 4.5 h post infusion, bacteria multiplied and began to fill the tubule lumen (arrow). As bacteria continue to multiply (8.5 h), epithelial linings disintegrate, shown by the lack of proximal tubule specific labelling (arrows). A single glomerular loop showed signs of dysfunction by slowing RBC flow (arrowhead). B. Real-time visualization shows that capillary blood flow remained constant around a PBS-infused sham tubule (blue outline). C and D. The velocity of RBCs within single peritubular capillaries is shown for infected (C) and sham nephrons (D). Data were achieved using a line scan method, where the axial view of a capillary was recorded every 2 ms in the multiphoton microscope for a defined time period. The slope of the RBCs (represented as black streaks within the red, dye-containing lumen of the vessel) within each vessel was determined and used to quantify the velocity ($\mu\text{m s}^{-1}$) of RBCs. For details of capillary selection and velocity measurements, see legend to Fig. S1. Scale bars = 30 μm .

the infected nephron, demonstrated that the area of low PO_2 , visible macroscopically by its white colouration, was localized within 1–2 nephrons from the site of infusion (data not shown).

Drop in PO_2 is caused by proximal tubule cells' rapid response to infection

To investigate the drop in tissue PO_2 occurring within the first hour of infection, prior to stoppage of blood flow, *in vitro* cell experiments were performed with freshly prepared primary rat proximal tubule cells (PTCs) (Uhlen *et al.*, 2000). Using the BD oxygen biosensor system, a significant increase ($P < 0.01$) in oxygen consumption was observed in infected PTCs, while the bacterial inoculum

itself [10^5 colony forming units (cfu) LT004] showed no discernible response (Fig. 2C). This eliminates the role of bacteria in consumption of oxygen; rather it indicates that the increased oxygen consumption is due to increased metabolism in infected PTCs. As known cellular responses to infection include the production of pro-inflammatory cytokines (Sansone, 2006), transcriptional changes of a subset of pro-inflammatory mediators were investigated (Fig. 2D). qRT-PCR revealed that exposure of PTCs to LT004 for 1 h elicited an upregulation of TNF- α and IL-1 β but not IL-6. After 5 h of infection, however, the PTCs did express IL-6, showing that this response occurred with altered kinetics as compared with TNF- α and IL-1 β . Within the infected tissue, transcriptional upregulation of TNF- α , IL-1 β and IL-6 was observed 5 h post infusion.

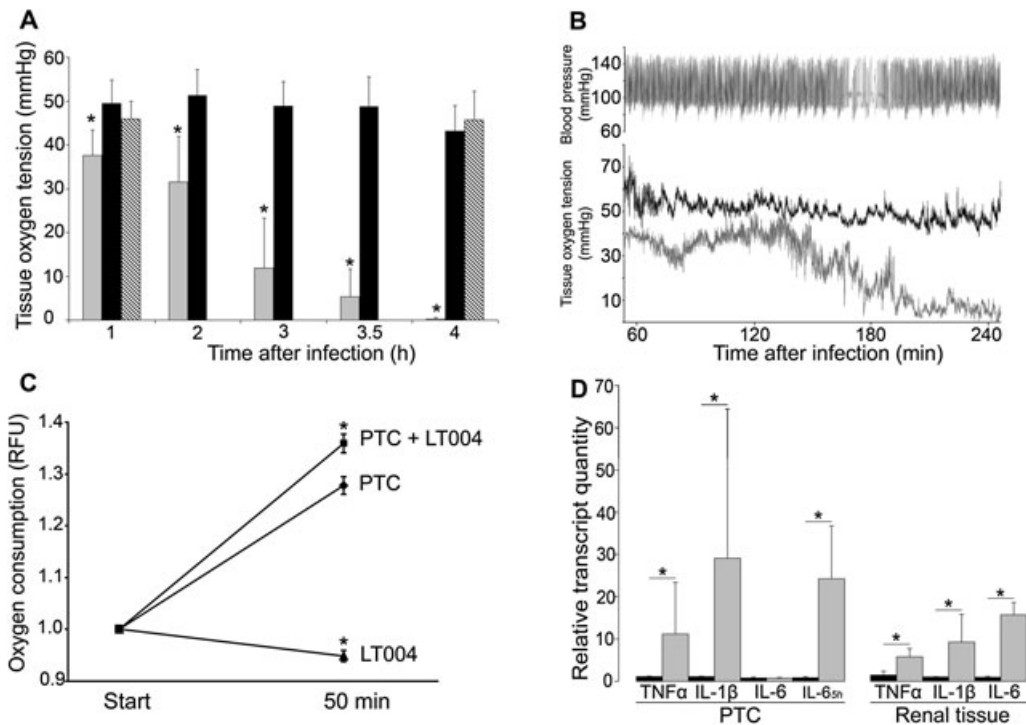


Fig. 2. Tissue oxygen tension during infection.

A. Measurements of PO₂ (mmHg) within infected (grey), PBS sham (black) and untouched (striped) renal cortex over 4 h ($n = 7$). Values are given as mean + SD. The asterisks indicate significant difference ($P < 0.05$).

B. Continuous recordings of arterial blood pressure (top) and tissue PO₂ (bottom) of an infected (grey) and a sham (black) nephron within an individual animal.

C. O₂ consumption, measured in relative fluorescent units (RFU) over 50 min, by sham infected PTCs ($n = 39$), infected PTCs (PTC + IT004) ($n = 39$) and by 10⁵ cfu bacteria (LT004) ($n = 16$). The asterisks indicate significant difference ($P < 0.01$) from sham infected PTCs.

D. qRT-PCR demonstrating the effect of LT004 infection (grey) and control PBS (black) on transcription of pro-inflammatory cytokines from isolated PTCs at 1 h. Data for IL-6 are shown for both 1 h and 5 h as indicated. Similarly, the pro-inflammatory cytokine profile from dissected renal tissue at 5 h is presented (black bars = PBS sham-injected tissue; grey bars = IT004-infected tissue). Values are given as mean + SD of experimental triplicates from three to four PTC preparations or infected rats. The asterisks indicate significant levels of upregulation ($P < 0.05$).

Infection-mediated actin re-arrangement resembles ischaemic injury and leads to epithelial breakdown

The dramatic decrease in PO₂ and shutdown of peritubular capillary flow suggested that initiation of the bacterial infection process induces a local, severe, ischaemic injury. In comparative experiments, a unilateral renal pedicle clamp was used to induce whole-kidney ischaemia. The resulting actin re-arrangement within proximal tubule cells was compared with infected nephrons 8 h post infusion by fixed-tissue confocal microscopy. In the ischaemic kidneys, F-actin staining of the proximal tubule microvilli was considerably reduced and blebbing of the apical membrane occurred (Fig. 3A and B). A similar pattern was observed in infected tubules, identified as proximal by the endocytosis of a small molecular weight dextran, revealing complete destruction of the F-actin rich microvilli (Fig. 3C and D). Neighbouring, non-infected tubules displayed strong microvilli staining, highlighting the localized nature of the cellular injury. Data from ascending infections demonstrate a similar pattern of

brush border loss and epithelial breakdown, as shown in Fig. S2.

Ischaemia-induced actin re-arrangement has been linked to the re-localization of membrane-bound integrins, causing a breakdown in epithelial barrier function (Molitoris and Marrs, 1999; Goldfarb *et al.*, 2002) and detachment of epithelial cells from the tubular basement membrane (Goligorsky *et al.*, 1993). To analyse the effect of infection-induced ischaemia on epithelial integrity, a single infected tubule was monitored by multiphoton microscopy (Fig. 3E). At 2 h post infusion, few bacteria were present within the tubule lumen, the epithelial barrier was intact and blood was flowing through peritubular capillaries. An increase in bacterial load over the ensuing hours was accompanied by a complete shutdown of blood flow in surrounding capillaries (Fig. 3E, 4.5 h). At later time-points signs of epithelial breakdown were evident, with large spherical entities outlined by the proximal tubule cell-specific dextran marker seen detached within the tubule lumen (Fig. 3E, 6 h). Breakdown of the epithelium was also indicated

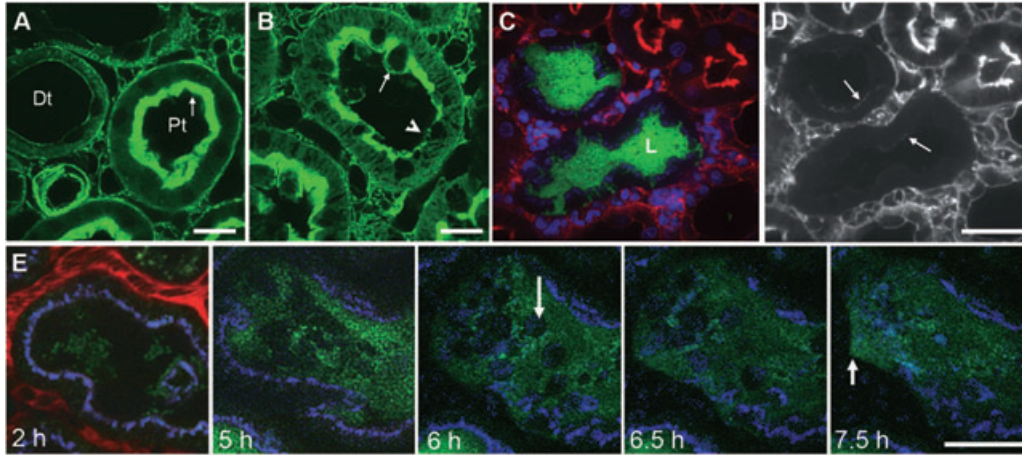


Fig. 3. Effects of ischaemic injury on tissue homeostasis.

A. Fixed tissue confocal microscopy shows intense phalloidin staining (green) of actin-rich apical microvilli in proximal tubule (Pt), but not distal tubule (Dt) cells.

B. Phalloidin staining reveals that membrane blebbing (arrow) and loss of microvilli (arrowhead) occurred 25 min post pedicle clamp-induced ischaemia.

C. Bacterial infection of a proximal tubule 8 h post infusion. Hoechst 33342 (blue) was used to label all cell nuclei including recruited immune cells. Bacteria (green) filled the tubule lumen (L).

D. Red channel from (C) separated and shown in grayscale. Destruction of apical microvilli was evident [arrows in (D) indicate the lack of intense microvilli phalloidin (grey) staining].

E. Progression of epithelial breakdown recorded in real-time by multiphoton microscopy. During the time-course of infection, numbers of bacteria (green) increased in the infected tubule (outlined by blue small dextran). Between 2 and 5 h post infection, the blood flow (visualized in red by large dextran) stopped in surrounding capillaries. Epithelial breakdown was apparent 6 h post infection. Large, cascade blue-labelled entities (arrow, 6 h) were present in the tubule lumen, representing either membrane blebs or sloughed epithelial cells. At 7.5 h post infection, gaps were seen in the blue labelled epithelial lining (arrow, 7.5 h). Scale bars: A, B = 10 μ m; D, E = 30 μ m.

by gaps between dextran-labelled tubular cells (Fig. 3E, 7.5 h; Fig. 1A, 8.5 h).

Tubular basement membrane hinders bacterial dissemination following epithelial breakdown

Breakdown of epithelial barrier integrity opened the possibility for unrestrained bacterial spread throughout the tissue, but the contrary was observed. At later stages of infection (8 h), when epithelial cells had begun to slough and disassociate, bacteria were found on the basal side of the proximal tubules cells (Fig. 4A). Observations of fixed tissues frequently showed large numbers of bacteria breaching the epithelial lining, in what appeared to represent paracellular movement (Fig. 4B). Bacterial passage between epithelial cells was verified using phalloidin staining to outline cell boundaries (Fig. 4C). Further spread of bacteria into the interstitium, however, appeared to be hindered, with bacteria restrained within the tubule space (Fig. 4B and C). Staining for collagen IV, the major component of tubular basement membrane, revealed that an intact basement membrane contained the bacteria within the tubule, thus functioning as an extra impediment to dissemination (Fig. 4D). These observations were corroborated using multiphoton microscopy of the living tissue (Fig. 4E and F, and Fig. 3E, 7.5 h),

showing apparent bacterial breach and containment, despite the loss of the dextran-labelled epithelial barrier.

Bacterial containment to the infected nephron by clotting

Early in the infection process, during the development of peritubular capillary dysfunction, small black silhouettes were seen aggregating in capillaries surrounding infected tubules (Fig. 5A). Their size indicated they were too small to be RBCs or infiltrating immune cells, suggesting they may be platelets. Within these capillaries large black (non-fluorescent) aggregates could be seen adhering to the vascular wall. Plasma, essentially devoid of RBCs, was seen beyond these obstructing masses. This plasma was identified by the intense solid red colour of the fluid-phase dextran marker.

To investigate the relevance of this observation, qRT-PCR was performed on RNA extracted specifically from infection sites both at 5 and 8 h post infusion (Fig. 5B). As early as 5 h post infusion, a few clotting cascade genes were upregulated including *Fgb* (Fibrinogen β), *Tfpi2* (Tissue factor pathway inhibitor) and *Selp* (P selectin). At 8 h, more genes were significantly upregulated including *Selp*, *Tfpi2*, *F3* (Tissue factor), *Serpine1* (Plasminogen activator inhibitor-1), *Fgb* and *Fgl2* (Fibrinogen like-2) (Fig. 5B). The finding of upregulation of both *Tfpi2* and *F3*

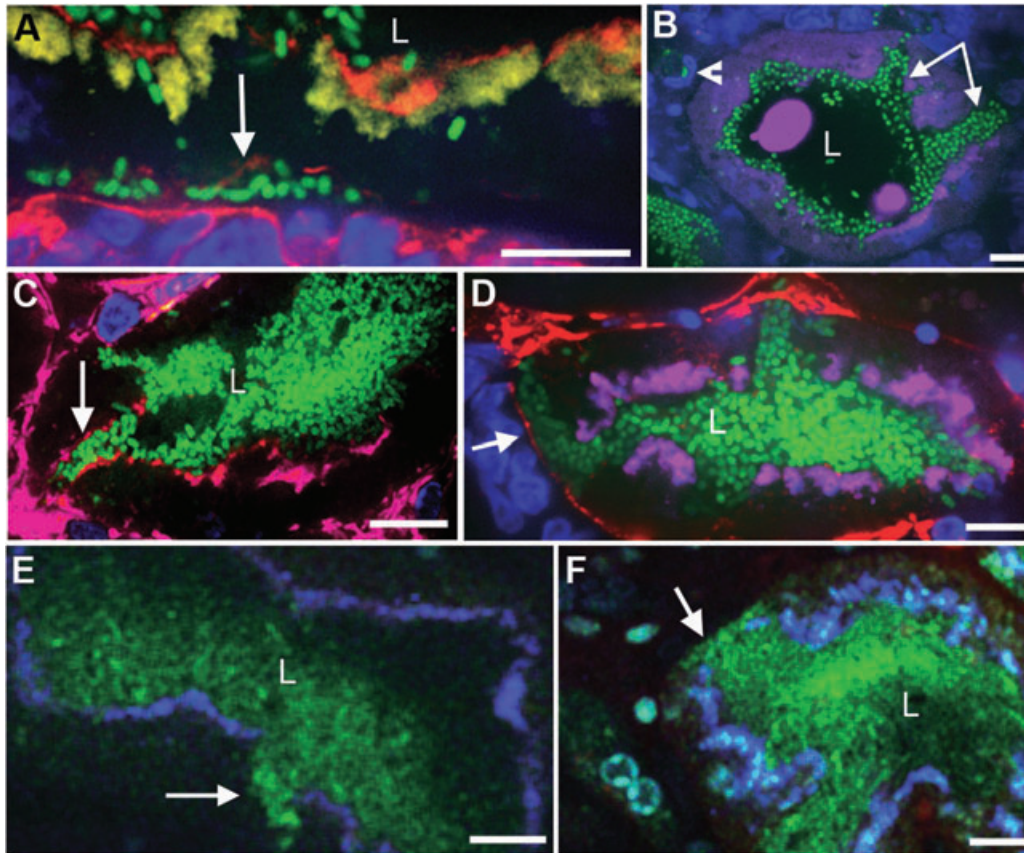


Fig. 4. Bacterial spread following epithelial breakdown.

A–D. Confocal imaging of fixed tissue 8 h post infusion.

A. Bacteria (green) are located on the apical as well as basolateral side of PTCs. The apical membrane is outlined by endocytosed small molecular weight dextran (yellow). Phalloidin stained actin (red) delineates the basal side of PTCs (arrow). L = lumen of proximal tubule.

B. A proximal tubule specific dextran (purple) lines the passage of bacteria, revealing paracellular migration of bacteria (arrows). The intense, dextran-labelled spherical entities seen in the tubule lumen represent either apical membrane blebs or sloughed epithelial cells. Recruited PMNs (blue nuclei) were occasionally seen actively engulfing disseminating bacteria (arrowhead).

C. Paracellular bacterial passage (arrow) shown with Phalloidin stained actin (pink).

D. An intact tubule basement membrane, shown by staining for collagen IV (red), hindered bacterial dissemination following epithelial breakdown (arrow).

E and F. Live multiphoton imaging showed bacteria breaching (arrow in E) the proximal tubule epithelial barrier (blue), and bacteria maintained within the tubule despite the loss of the epithelial lining (arrow in F). Scale bars = 10 μ m.

is not entirely unexpected as both have been shown to be upregulated post-thrombin generation, an essential factor in clot formation (Neaud *et al.*, 2004). Markers of hypoxia such as *Angptl4* [angiopoietin-like 4 (Le Jan *et al.*, 2003)] and *Vegf* (vascular endothelial growth factor) were also investigated, showing a significant upregulation of *Angptl4* but not *Vegf*.

The effect of local clotting could be seen at 24 h post infusion within the foci of inflammation (Fig. 5C). Live imaging of the site shows normal blood flow in peritubular capillaries surrounding the inflammation foci but not within, delineating the border to healthy tissue. There was a large infiltration of immune cells to the site and tissue morphology in the area was disrupted. No visible bacteria remained at the site. Higher magnification of the border of

an infection site (Fig. 5D) shows blood flowing through surrounding vessels but stopping abruptly at the edge.

Although the role of clotting is well described for blood-borne infections, the physiological role of clotting in ascending UTI, where the bacteria are localized at the mucosal linings, is currently unknown. To address this, we applied anticoagulant therapy. Following bacterial infusion, animals ($n=3$) were treated with heparin sodium. A representative selection of images demonstrating the altered time-course of infection is shown as Fig. 6A. Treatment with heparin delayed the shutdown of blood flow through peritubular capillaries (for a comparison to non-heparin treated, infected animals see Fig. 1A). Some capillaries showed normal blood flow as

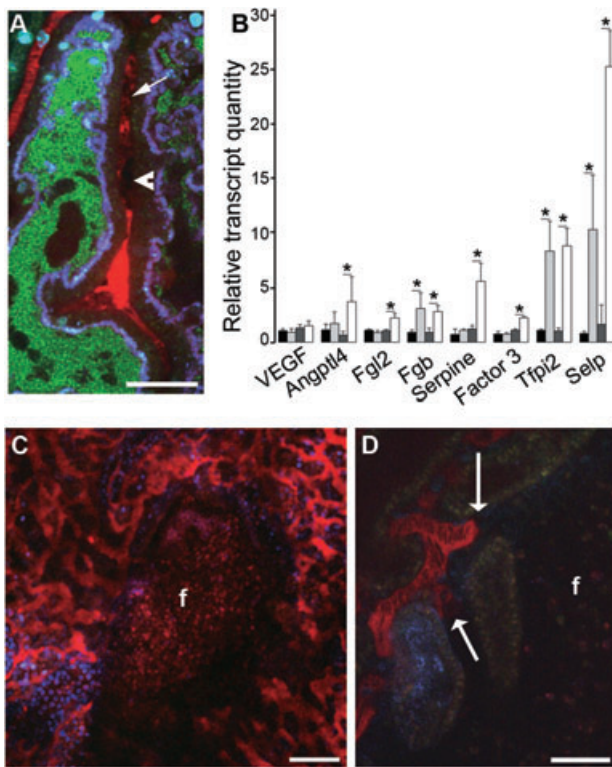


Fig. 5. Blood clotting in mucosal infections. **A.** Live multiphoton imaging shows black silhouettes (arrow), indicative of platelets, within the blood vessels (red) surrounding an LT004-infected (green) proximal tubule (blue) 2.5 h post infection. Black masses adhering to the wall of the vessel (arrowhead) suggest platelet aggregates. A lack of RBC movement is seen in the area. Scale bar = 30 μ m. **B.** Changes in mRNA levels of indicated genes from tissue isolated 5 h (black = PBS, light grey = IT004) and 8 h (dark grey = PBS, white = IT004). Numbers are determined by qRT-PCR and normalized to endogenous control *Gapdh* mRNA levels. Each bar denotes the mean + SD of three rats. The asterisks indicate significant levels of upregulation ($P < 0.05$). **C.** A 3D projection of a 10 μ m stack showing an infection foci (f) 24 h post infusion. Scale bar = 100 μ m. **D.** Edge of a 24 h infection foci (f) showing the abrupt stoppage of blood flow (arrows). Scale bar = 30 μ m.

late as 5.5 h post infusion, but ultimately the RBC flow stopped. Line scan data supported the delay, but not complete prevention, of vascular shutdown (Fig. 6B). Heparin-treated animals suffered from a sharp drop in blood pressure, and had to be sacrificed 6–8 h post infusion. As hypotension is characteristic of sepsis, blood and selected organs were analysed for the presence of bacteria. Large numbers of bacteria were found within the blood, as well as the heart, liver and spleen (Fig. 6D). This is in contrast to negative cultures taken from all other 8 h infected animals, not treated with heparin, included in this study ($n = 20$). These data suggest that inhibition of the clotting cascade promotes systemic spread of bacteria, urosepsis.

Discussion

Ascending pyelonephritis is known to cause major alterations in cortical tissue homeostasis. Here we employ a real-time kidney infection model to provide morphological, physiological and molecular details of infection-associated events that have severe consequences on renal function as depicted schematically in Fig. 6D.

Using this model we have noted that a striking effect of UPEC infection is the rapid induction of vascular dysfunction. Despite the localization of bacteria within the tubule lumen, blood flow in peritubular capillaries stopped within hours of infection. Previous studies in longer-term ascending pyelonephritis models have recognized the disruption of renal vasculature using techniques such as microangiographs and electron microscopy (Hill, 1989). PMN plugs and preglomerular vasospasm have been implicated in these models as possible mechanisms for this dysfunction (Hill, 1989; Ivanyi, 1991; Ronald and Nicolle, 2002). In our model stoppage occurred prior to the infiltration of PMNs, while blood flow through the adjacent glomerulus was maintained, limiting the role of an upstream vasoregulatory event.

The rapidity of the drop in cortical PO_2 following bacterial infusion implies that events other than loss of blood flow are involved in regulating PO_2 homeostasis. Our data revealed that infected primary PTCs displayed enhanced oxygen consumption within the same time frame as they upregulated expression of pro-inflammatory cytokines *in vitro*. These data confirm the rapid immune accessory functions of PTCs (Jevnikar *et al.*, 1991) in sensing and responding to infection, which was also confirmed *in vivo*. Expression of these cytokines may also indicate a possible mechanism by which clotting is initiated from the epithelium to induce endothelial activation. This also suggested a possible mechanism for increased cellular metabolism. The rapid metabolic increase may represent the onset of the inflammatory response following this large stimulus. The early drop in PO_2 was soon followed by a complete loss, indicating a hypoxic environment in a limited area surrounding the infection. Our unsuccessful attempts to detect HIF-1 α and VEGF in the tissue (data not shown), along with a lack of *Vegf* transcript indicated no VEGF-dependent angiogenesis occurring within the first 8 h (Liao and Johnson, 2007). The cleared infection site at 24 h also showed little sign of re-vascularization.

Hypoxia, in conjunction with substantial re-arrangement of the actin cytoskeleton in epithelial cells lining the infected tubule, indicated that infection caused a highly localized ischaemic injury. Renal pedicle clamp models have demonstrated the numerous effects of ischaemia on tissue structure and function. The rapid re-arrangement of cortical actin cytoskeleton in ischaemia (Schwartz *et al.*, 1999; Ashworth *et al.*, 2001) alters the interactions

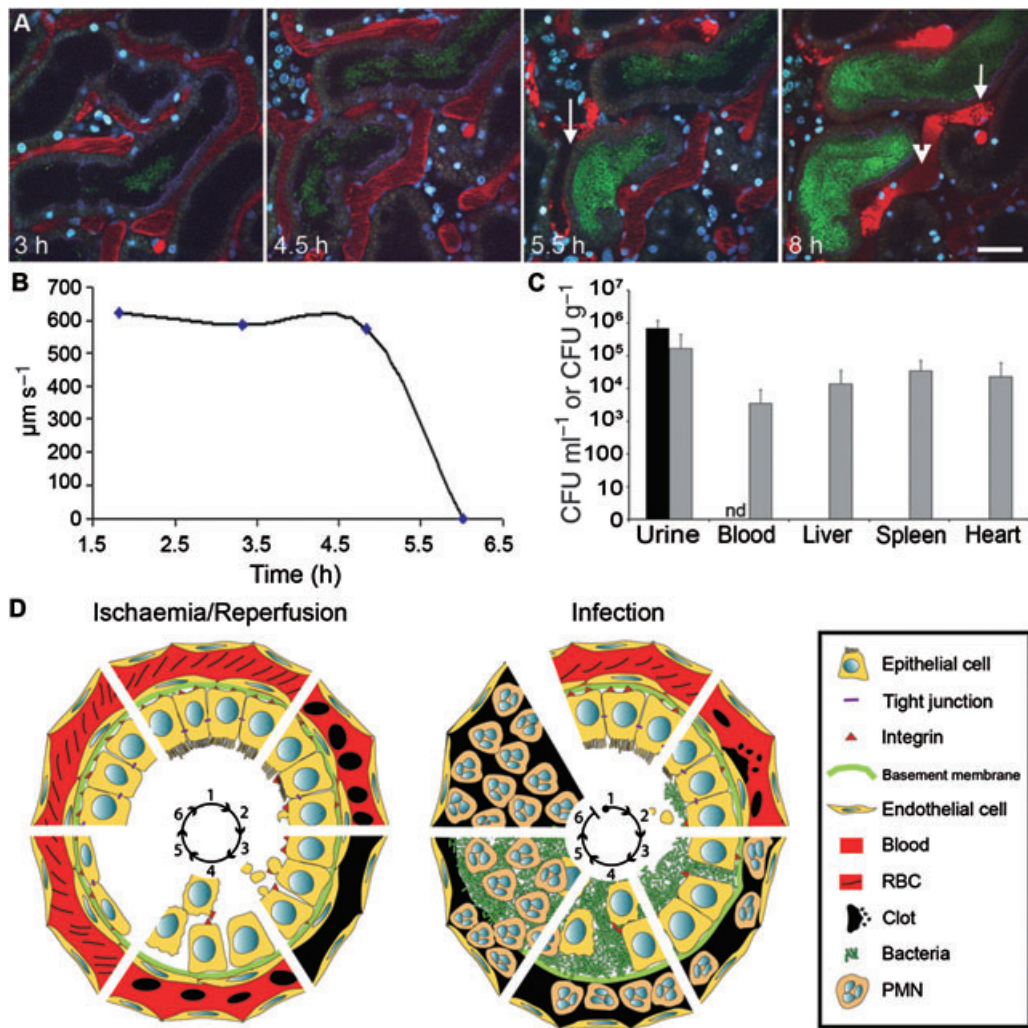


Fig. 6. Heparin treatment affects clotting, leading to bacterial dissemination and urosepsis.

A. Representative progression of infection in a rat treated with heparin sodium, recorded in real-time by multiphoton microscopy. Blood (red) flowed freely up to 4.5 h post infection despite bacterial presence (green). Some vessels (arrow) show signs of dysfunction at 5.5 h. RBC flow stopped in certain surrounding vessels (arrowhead, 8 h) and aggregation of platelets was observed (arrow 8 h). Hoechst 33342 = cell nuclei (light blue). Scale bar = 30 μm .

B. RBC flow within a selected capillary of the heparin-treated infected rat shown in (A).

C. Bacterial numbers within the urine, blood and organs of heparin-treated infected animals (grey bars) ($n = 3$). Black bars represent infected rats without heparin treatment ($n = 20$). nd = not detectable. Values are given as mean + SD.

D. Cartoon comparing the events occurring in ischaemia/reperfusion (left) and in infection (right). In ischaemia/reperfusion (left) normal tissue (1) quickly begins to change following the slowing/stoppage of blood flow, with loss of polarity and tubular cell brush border, causing blebbing (2). As the ischaemia progresses the cells loose contact with the basement membrane and each other (3). At the beginning of reperfusion, sloughed tubular cells may cause obstruction of the tubule (4). As blood flow re-establishes, surviving cells begin to re-epithelialize the basement membrane (5), from where they de-differentiate back into functional, tight tubular epithelium (6). In infection (right) normal tissue (1), quickly colonized by bacteria, begins to show hallmarks of ischaemia with brush border/polarity loss and blebbing accompanying the initiation of clotting (2). The ischaemic injury advances as bacteria multiply. This, together with the initial arrival of PMNs disrupts the epithelial lining, allowing paracellular migration of bacteria. The fate of the endothelium is currently unknown (3). Due to the integrity of the basement membrane, bacteria are maintained within the tubular lumen although the epithelial cells are sloughed (4). As the infection progresses, numerous PMNs infiltrate the tissue and migrate into the tubular lumen (5). Within 24 h, bacteria are cleared by massive numbers of PMNs, which destroy the tissue morphology and leaves a renal scar (6).

between the microfilament system, integrins, immunoglobulins and cell adhesion molecules. Interference with the essential cell–cell and cell–extracellular matrix adhesion leads to disruption of tubular integrity (Molitoris, 1991; Goligorsky *et al.*, 1993; Molitoris and Marrs, 1999).

Sloughing of epithelial cells into the lumen of proximal tubules resulted in a denuded basement membrane, allowing for unrestricted backleak of tubular fluid (Goligorsky *et al.*, 1993). The subsequent alteration in intrarenal haemodynamics is a feature of both ischaemic injury and

acute renal failure (Goldfarb *et al.*, 2002). Our observations suggest that infection-induced renal scarring occurs due to a combination of factors including ischaemic injury and its numerous consequences.

Sloughing of the single layer of proximal tubule epithelia also has major implications for bacterial dissemination. In contrast to bladder epithelium, reported to act as a bacterial reservoir in recurrent infections (Mulvey *et al.*, 1998; Mulvey *et al.*, 2000; Bower *et al.*, 2005), sloughing of the tubule epithelium implies that bacterial internalization would not be beneficial for persistence in the kidney. Loss of tubular integrity was also found to enable paracellular movement of UPEC. While tubular basement membrane does not impede fluid transport, it appears to hinder immediate bacterial dissemination into the interstitium. This delay in spread may be beneficial to the host, giving it time to stop local blood flow and recruit PMNs. The loss of tubular integrity may also be advantageous in allowing PMN access to the tubular lumen (Ivanyi *et al.*, 1983; Hill, 1989).

During the course of infection, bacteria were contained to the infection site and at 24 h were cleared. In blood-borne infections containment is commonly achieved by rapid activation of clotting via endothelial activation. The role of thrombosis formation to 'wall off' an infection to prevent dissemination has been described (Sun, 2006). Our model indicates a similar clotting process, but in the absence of wounding, endothelial disruption, immune cell recruitment and bacterial–blood interaction. This highlights the role of cell–cell signalling in inducing an indirect effect on local vasculature. The production of pro-inflammatory cytokines, such as TNF- α , by tubular epithelia may trigger activation of local endothelium. Activation leads to a pro-coagulant surface and synthesis of tissue factor, thereby promoting clotting in surrounding capillaries (Hack and Zeerleder, 2001). The single layer epithelium in the kidney separating the mucosal infection and the bloodstream would allow for this rapid signalling event while identifying the need for such a defence mechanism. The formation of such a clearly defined infection foci highlights the role of clotting in isolating the infection.

Heparin treatment of infected animals caused a significant delay in the shut-down of blood flow in local capillaries, confirming the role of clotting in the process. Treatment also caused urosepsis with fatal consequences, signifying a novel role for clotting as a member of the host's innate defence mechanisms against mucosal pathogens. Detailed molecular knowledge of this mucosal infection-induced clotting is currently incomplete. The short time frame of capillary shutdown indicates a mechanism independent of inflammatory cell recruitment. The ischaemic injury appears to be multifactorial of nature, with heparin treatment resulting in incomplete prevention of capillary shutdown, and a rapid drop in PO₂ occurring

prior to clotting. The combination of these factors leads to a rapid onset of ischaemia, which both helps and harms the host. Ischaemia appears to facilitate isolation and clearance of the infection but subsequently causes local renal scarring; the balance between these factors being decisive in infection outcome.

The implications of ischaemia-mediated protection from urosepsis may be relevant in developing new treatment regimes. Systemic delivery of antibiotics may be suboptimal, with impaired blood flow limiting accessibility to the infection site. The risks of increased bacterial translocation may also need to be weighed against the risks of systemic coagulation in septic patients undergoing anticoagulant therapy. These observations illustrate the importance of integrating molecular studies of bacterial pathogenesis with the physiological effects infection exerts on host tissue. Intravital imaging exposes dynamic and multifactorial aspects of infection unattainable in cell cultures and sacrificed animals. In combination with detailed molecular studies, intravital imaging has great potential for the future understanding of pathogenesis.

Experimental procedures

Bacteria and animals

The clinically derived UPEC strain LT004 (CFT073, *cobS:: Φ (P_{LtetO-1}-gfp⁺), cmr^r; O6:K2:H1) (Mansson *et al.*, 2007) was cultivated in Luria–Bertani (LB) medium at 37°C, shaking, in the presence of chloramphenicol (20 μ g ml⁻¹). cfu from urine, blood and tissue were obtained by dilution plating on LB agar plates containing chloramphenicol. Male Munich-Wistar (255 \pm 22 g) (Harlan, Indianapolis, IN, USA) or Sprague-Dawley (264 \pm 16 g) (Scanbur BK, Sweden) rats with free access to chow and water were used. Retrograde infections were performed as previously described (Mansson *et al.*, 2007). Studies were performed in accordance with the National Institutes of Health's *Guide for the Care and Use of Laboratory Animals* and have been approved by the Institutional Animal Care and Use Committee (Indianapolis, IN, USA), the animal ethics committee at Uppsala University (Sweden) or Stockholms Norra Djurförsöksetiska Nämnd.*

Surgical preparation

Rats were anaesthetized by intraperitoneal injection of 130–150 mg kg⁻¹ thiobutabarbital (Inactin) (Sigma, St Louis, MO/Sigma, Sweden). For multiphoton imaging, animals underwent a tracheotomy and cannulation of femoral artery for measurement of arterial blood pressure, femoral vein for infusion of 0.9% saline (1.5 ml h⁻¹), and jugular vein for infusion of dyes and removal of blood samples. For measurement of PO₂ and collection of tissue for mRNA analysis, animals had a tracheostomy and cannulation of the femoral artery, femoral vein and left ureter. Renal clamp ischaemia experiments were performed as previously described (Ashworth *et al.*, 2001). Core body temperature was monitored rectally and maintained using heating pads. For 24 h experiments rats were anaesthetized by intraperitoneal

injection of 40–50 mg kg⁻¹ sodium pentobarbital, in the absence of the tracheostomy and cannulation. For imaging rats were transferred from sodium pentobarbital to halothane/oxygen anaesthesia, allowing fine-tuning and recovery overnight. On day 2 rats were prepared for imaging as described above.

Micro-perfusion procedures

Infection by tubular microperfusion was performed as previously described (Mansson *et al.*, 2007). In brief, fresh LT004 was cultivated to OD₆₀₀ of 0.6 and concentrated to 10⁹ cfu ml⁻¹ in PBS⁺ (PBS with 1 mM CaCl₂ and 2 mM MgCl₂) containing 1 mg ml⁻¹ Fast Green FCF (Fisher, Fair Lawn, NJ, USA) and 0.2 mg ml⁻¹ cascade blue-conjugated 10 kDa dextran (Molecular Probes, Eugene, OR, USA). This preparation did not alter the neutral pH. Bacterial suspensions or control PBS was aspirated into sharpened micropipettes filled with heavy mineral oil. The left kidney was exposed via a subcostal flank incision, freed from surrounding fat, and supported in a kidney cup. Under stereoscopic microscope observation (96×), the bacterial suspension was infused over a period of 10 min into the lumen of superficial proximal tubules using a Leitz micromanipulator and either a mercury levelling bulb or microinfusion pump. Bacteria/PBS was infused at an average rate of 54 nl min⁻¹ using the mercury bulb and 40 nl min⁻¹ using the microinfusion pump. This corresponded to delivery of 3–6 × 10⁵ cfu per injection. To allow for localization of injection sites, Sudan black-stained castor oil was injected into nearby tubules.

Multiphoton microscopy

All multiphoton imaging was performed using the set-up previously optimized and described (Mansson *et al.*, 2007). Images were collected using a Bio-Rad MRC 1024 confocal/2-photon system (Bio-Rad, Hercules, CA, USA) attached to a Nikon Diaphot inverted microscope (Fryer, Huntley, IL, USA) with either a Nikon ×60 1.2-NA water-immersion or a 20× objective. Fluorescence excitation was provided by a Tsunami Lite titanium-sapphire laser (Spectraphysics, Mountain View, CA, USA). Image stacks were collected in 1 μm optical steps into the tissue at a depth of approximately 30–100 μm using an excitation wavelength of 810 nm and neutral density filters set to 25–40%. Fluorescent probes were injected as a single bolus via a jugular vein access line. Tetramethylrhodamine-conjugated 500 kDa dextran (~2.5 mg per 400 μl 0.9% saline, Molecular Probes, Eugene, OR) was used to visualize blood flow and Hoechst 33342 (~600 μg per 0.4 ml of 0.9% saline, Molecular Probes, Eugene, OR) to stain cell nuclei. Rats were placed on the microscope stage with the exposed kidney positioned in a 50 mm-diameter coverslip-bottomed cell culture dish (Warner Instruments, CT, USA) containing isotonic saline. Line scan measurements were performed as previously described (Kleinfeld *et al.*, 1998).

Measurement of in vivo renal oxygen tension

All measurements were performed as previously described (Palm *et al.*, 2003). Briefly, following microperfusion, renal PO₂ was measured using modified Clark-type microelectrodes (4–6 μm o.d., Unisense, Aarhus, Denmark; Liss *et al.*, 1997). The electrodes were two-point calibrated in water saturated with either

Na₂S₂O₅ or air at 37°C. Microelectrodes were then inserted into the lumen of the infused nephrons using a micromanipulator, under stereoscopic microscope observation. Simultaneous measurements of bacteria- and PBS-infused nephrons were conducted for a total of 240 min after microperfusion.

Measurements of oxygen consumption in vitro

Primary PTCs were isolated for O₂ consumption measurements as previously described (Korner *et al.*, 1994; Palm *et al.*, 2003). O₂ consumption was determined using the 384-well BD oxygen biosensor system (BD Biosciences, Sweden) at 37°C as described (Schieke *et al.*, 2006). Appropriate cell concentrations were determined prior to reading, in order to reach maximum fluorescence signal after 60–80 min. O₂ consumption was recorded in PTCs infected with 10⁵ cfu LT004 (*n* = 39), in non-infected PTCs (*n* = 39) as well as from 10⁵ cfu LT004 (*n* = 16). Cells from four separate tissue preparations were used. Plates were read from the bottom using a microplate reader (Safire II, Tecan Austria GmbH, Grödig, Austria) (485 ± 10 nm excitation, and 630 ± 10 nm emission). Data were normalized to background fluorescence and expressed as relative fluorescent units according to manufacturers' instructions.

Immunohistochemistry

After multiphoton imaging, kidneys were removed, fixed with 4% paraformaldehyde (Merck, Germany), and frozen in Tissue-tek (Sakura, the Netherlands). The tissue could then be further analysed *ex vivo*, as the physiological nature of the living models prevents the use of antibodies and some stains. Tissue slices (10 μm thick) were prepared for confocal microscopy (Richter-Dahlfors *et al.*, 1997). Actin was detected using phalloidin conjugated with either TRITC or Texas Red (Sigma, Germany, and Molecular Probes, OR). Cell nuclei were labelled with Hoechst 33342 dye (Molecular Probes, OR). Antibodies used were Rbα-Collagen IV (Abcam, UK), and GtαRb-Cy3 (Jackson, USA). Confocal microscopy was performed using an UltraVIEW RS-3 laser confocal system with microlens-enhanced Nipkow discs (CSU21; Perkin Elmer) mounted on a Zeiss Axiovert microscope equipped with a Hamamatsu ORCA ER cold CCD camera.

Image processing

Images and data volumes were processed using Metamorph Image Processing Software (Universal Imaging-Molecular Devices, PA, USA), UltraVIEW ERS (PerkinElmer, MA, USA) and ImageJ (US National Institutes of Health, MD, USA, <http://rsb.info.nih.gov/ij/>). Final figures were prepared with Adobe Photoshop (Adobe, CA, USA).

Quantitative real-time PCR

The renal infection site was dissected using a 5 mm biopsy punch, medullar tissue was removed, and total RNA extraction was performed on the resulting ~30 mg tissue using Trizol (Invitrogen, Sweden). Experimental quadruplicates were performed on three separate preparations for both infected and non-infected samples. Alternatively, total RNA was extracted from primary

PTCs exposed for 1 h to LT004 or PBS ($n = 3$). cDNA was transcribed from 1 μg of RNA using the SuperScript III First Strand Synthesis Supermix kit (Invitrogen, Sweden). qRT-PCR was performed using a 7500 Real Time PCR System (Applied Biosystems, Sweden) and the Power SYBR Green PCR Mastermix (Applied Biosystems, Sweden). In all experiments GAPDH was used as an endogenous reference gene. Primer sequences can be found in Table S1.

Heparin treatment

Immediately following microperfusion and surgical preparation for multiphoton microscopy, rats were treated with 400 U kg^{-1} of heparin sodium via the jugular venous access line (within 30 min of infection). After 4 h, a second dose (200 U kg^{-1}) was administered. Following sacrifice, the liver, spleen and heart were aseptically removed, homogenized in PBS and analysed for bacterial cfu. Blood samples were taken throughout the experiment to confirm lack of clotting and analysed for bacterial cfu.

Data analysis

Normally distributed data are presented as mean and standard deviation. One-tailed Student *t*-test was used to evaluate significance. Differences of $P < 0.05$ were considered significant. Alterations in tubular PO_2 was analysed using paired statistics (paired *t*-test). Relative O_2 consumption was analysed using non-parametric statistics ANOVA (Kruskal–Wallis) followed by Dunns *post hoc* test.

Acknowledgements

The authors wish to thank Dr SB Campos for valuable surgical assistance. This work was supported by Anders Otto Swärds Stiftelse, Ulrika Eklunds Stiftelse and Svenska Läkaresällskapet (KM), the Marie Curie Early Stage Research Training Fellowship of the European Community's Sixth Framework Programme (MEST-CT-2004–8475), the Swedish Research Council, the Royal Swedish Academy of Sciences (ARD), and National Institutes of Health Grants P01 DK-53465 and DK069408 (BAM). Live imaging data were generated at The Indiana Center for Biological Microscopy. No financial conflicts of interest apply to any of the authors.

References

Ashworth, S.L., Sandoval, R.M., Hosford, M., Bamburg, J.R., and Molitoris, B.A. (2001) Ischemic injury induces ADF relocalization to the apical domain of rat proximal tubule cells. *Am J Physiol* **280**: F886–F894.

Backhed, F., Soderhall, M., Ekman, P., Normark, S., and Richter-Dahlfors, A. (2001) Induction of innate immune responses by *Escherichia coli* and purified lipopolysaccharide correlate with organ- and cell-specific expression of Toll-like receptors within the human urinary tract. *Cell Microbiol* **3**: 153–158.

Bower, J.M., Eto, D.S., and Mulvey, M.A. (2005) Covert operations of uropathogenic *Escherichia coli* within the urinary tract. *Traffic (Copenhagen, Denmark)* **6**: 18–31.

Chassin, C., Hornef, M.W., Bens, M., Lotz, M., Goujon, J.M., Vimont, S., *et al.* (2007) Hormonal control of the renal immune response and antibacterial host defense by arginine vasopressin. *J Exp Med* **204**: 2837–2852.

Chromek, M., Slamova, Z., Bergman, P., Kovacs, L., Podracka, L., Ehren, I., *et al.* (2006) The antimicrobial peptide cathelicidin protects the urinary tract against invasive bacterial infection. *Nat Med* **12**: 636–641.

El-Achkar, T.M., Huang, X., Plotkin, Z., Sandoval, R.M., Rhodes, G.J., and Dagher, P.C. (2006) Sepsis induces changes in the expression and distribution of Toll-like receptor 4 in the rat kidney. *Am J Physiol* **290**: F1034–F1043.

Goldfarb, D.A., Nally, J.V., and Schreiber, M.J.J. (2002) Etiology, pathogenesis, and management of renal failure. In *Campbells Urology*, 8th edn. Walsh, P., Reitek, A., Vaughan, E., and Weir, A. (eds). Philadelphia, PA: Saunders, pp. 273–306.

Goligorsky, M.S., and DiBona, G.F. (1993) Pathogenetic role of Arg-Gly-Asp-recognizing integrins in acute renal failure. *Proc Natl Acad Sci USA* **90**: 5700–5704.

Goligorsky, M.S., Lieberthal, W., Racusen, L., and Simon, E.E. (1993) Integrin receptors in renal tubular epithelium: new insights into pathophysiology of acute renal failure. *Am J Physiol* **264**: F1–F8.

Hack, C.E., and Zeerleder, S. (2001) The endothelium in sepsis: source of and a target for inflammation. *Crit Care Med* **29**: S21–S27.

Hill, G.S. (1989) Renal infection. In *Uropathology*. Hill, G.S. (ed.). New York: Churchill Livingstone, pp. 333–429.

Ivanyi, B. (1991) Hypoxic damage to tubules due to blockage of perfusion in acute hematogenous *E. coli* pyelonephritis of rats. *Acta Morphol Hung* **39**: 239–248.

Ivanyi, B., Ormos, J., and Lantos, J. (1983) Tubulointerstitial inflammation, cast formation, and renal parenchymal damage in experimental pyelonephritis. *Am J Pathol* **113**: 300–308.

Jahnukainen, T., Chen, M., and Celsi, G. (2005) Mechanisms of renal damage owing to infection. *Pediatr Nephrol (Berlin, Germany)* **20**: 1043–1053.

Jevnikar, A.M., Brennan, D.C., Singer, G.G., Heng, J.E., Maslinski, W., Wuthrich, R.P., *et al.* (1991) Stimulated kidney tubular epithelial cells express membrane associated and secreted TNF alpha. *Kidney Int* **40**: 203–211.

Kleinfeld, D., Mitra, P.P., Helmchen, F., and Denk, W. (1998) Fluctuations and stimulus-induced changes in blood flow observed in individual capillaries in layers 2 through 4 of rat neocortex. *Proc Natl Acad Sci USA* **95**: 15741–15746.

Korner, A., Eklof, A.C., Celsi, G., and Aperia, A. (1994) Increased renal metabolism in diabetes. Mechanism and functional implications. *Diabetes* **43**: 629–633.

Langenberg, C., Bellomo, R., May, C., Wan, L., Egi, M., and Morgera, S. (2005) Renal blood flow in sepsis. *Crit Care (London, England)* **9**: R363–R374.

Le Jan, S., Amy, C., Cazes, A., Monnot, C., Lamande, N., Favier, J., *et al.* (2003) Angiopoietin-like 4 is a proangiogenic factor produced during ischemia and in conventional renal cell carcinoma. *Am J Pathol* **162**: 1521–1528.

Liao, D., and Johnson, R.S. (2007) Hypoxia: a key regulator of angiogenesis in cancer. *Cancer Metastasis Rev* **26**: 281–290.

Liss, P., Nygren, A., Revsbech, N.P., and Ulfendahl, H.R.

- (1997) Intrarenal oxygen tension measured by a modified Clark electrode at normal and low blood pressure and after injection of x-ray contrast media. *Pflugers Arch* **434**: 705–711.
- Mansson, L.E., Melican, K., Boekel, J., Sandoval, R.M., Hautefort, I., Tanner, G.A., et al. (2007) Real-time studies of the progression of bacterial infections and immediate tissue responses in live animals. *Cell Microbiol* **9**: 413–424.
- Molitoris, B.A. (1991) Ischemia-induced loss of epithelial polarity: potential role of the actin cytoskeleton. *Am J Physiol* **260**: F769–F778.
- Molitoris, B.A., and Marris, J. (1999) The role of cell adhesion molecules in ischemic acute renal failure. *Am J Med* **106**: 583–592.
- Mulvey, M.A., Lopez-Boado, Y.S., Wilson, C.L., Roth, R., Parks, W.C., Heuser, J., and Hultgren, S.J. (1998) Induction and evasion of host defenses by type 1-piliated uropathogenic *Escherichia coli*. *Science (New York, NY)* **282**: 1494–1497.
- Mulvey, M.A., Schilling, J.D., Martinez, J.J., and Hultgren, S.J. (2000) Bad bugs and beleaguered bladders: interplay between uropathogenic *Escherichia coli* and innate host defenses. *Proc Natl Acad Sci USA* **97**: 8829–8835.
- Neaud, V., Duplantier, J.G., Mazzocco, C., Kisiel, W., and Rosenbaum, J. (2004) Thrombin up-regulates tissue factor pathway inhibitor-2 synthesis through a cyclooxygenase-2-dependent, epidermal growth factor receptor-independent mechanism. *J Biol Chem* **279**: 5200–5206.
- O'Callaghan, C. (2006) *The Renal System at a Glance Oxford*. Oxford: Blackwell Publishing.
- Palm, F., Cederberg, J., Hansell, P., Liss, P., and Carlsson, P.O. (2003) Reactive oxygen species cause diabetes-induced decrease in renal oxygen tension. *Diabetologia* **46**: 1153–1160.
- Richter-Dahlfors, A., Buchan, A.M., and Finlay, B.B. (1997) Murine salmonellosis studied by confocal microscopy: *Salmonella typhimurium* resides intracellularly inside macrophages and exerts a cytotoxic effect on phagocytes *in vivo*. *J Exp Med* **186**: 569–580.
- Ronald, A.R., and Nicolle, L.E. (2002) Infections of the upper urinary tract. In: *Diseases of the Kidney and Urinary Tract*, 7th edn. Schrier, R.W. (ed.) Philadelphia, PA: Lippincott Williams and Wilkins, pp. 941–969.
- Sansonetti, P.J. (2006) The innate signaling of dangers and the dangers of innate signaling. *Nat Immunol* **7**: 1237–1242.
- Schaeffer, A.J. (2001) What do we know about the urinary tract infection-prone individual? *J Infect Dis* **183** (Suppl. 1): S66–S69.
- Schaeffer, A.J. (2002) Infections of the Urinary Tract. In: *Campbells Urology*, 8th, edn. Walsh, P., Reitk, A., Vaughn, E., and Wein, A. (eds). Philadelphia, PA: Saunders, pp. 515–602.
- Schieke, S.M., Phillips, D., McCoy, J.P., Jr., Aponte, A.M., Shen, R.F., Balaban, R.S., and Finkel, T. (2006) The mammalian target of rapamycin (mTOR) pathway regulates mitochondrial oxygen consumption and oxidative capacity. *J Biol Chem* **281**: 27643–27652.
- Schwartz, N., Hosford, M., Sandoval, R.M., Wagner, M.C., Atkinson, S.J., Bamburg, J., and Molitoris, B.A. (1999) Ischemia activates actin depolymerizing factor: role in proximal tubule microvillar actin alterations. *Am J Physiol* **276**: F544–F551.
- Smellie, J.M., Poulton, A., and Prescod, N.P. (1994) Retrospective study of children with renal scarring associated with reflux and urinary infection. *BMJ (Clinical research ed.)* **308**: 1193–1196.
- Sun, H. (2006) The interaction between pathogens and the host coagulation system. *Physiology (Bethesda, MD)* **21**: 281–288.
- Svanborg, C., Frendeus, B., Godaly, G., Hang, L., Hedlund, M., and Wachtler, C. (2001) Toll-like receptor signaling and chemokine receptor expression influence the severity of urinary tract infection. *J Infect Dis* **183** (Suppl. 1): S61–S65.
- Uhlen, P., Laestadius, A., Jahnukainen, T., Soderblom, T., Backhed, F., Celsi, G., et al. (2000) Alpha-haemolysin of uropathogenic *E. coli* induces Ca²⁺ oscillations in renal epithelial cells. *Nature* **405**: 694–697.

Supplementary material

The following supplementary material is available for this article online:

Fig. S1. Determination of blood flow using the line scan method.

A. White line denotes the capillary chosen for measurement of blood flow rates in the infected site seen in Fig. 1A. Measurements were taken 10 μm shallower than images in Fig. 1A.

B. A 1 s segment of the line scan from the reference picture (A) at 2.25 h post infusion. As RBCs do not take up the red fluid phase marker they appear as black streaks in the plasma. The diagram shows the calculation of the velocity of a single RBC.

C. A line scan of the same capillary as (B) at 4.5 h showing no flow.

D–F. Reference picture and line scans from the PBS sham site in Fig. 1B. Scale bars = 30 μm .

Fig. S2. Actin re-arrangement in an ascending infection. Confocal microscopy of a 4 day ascending infection with LT004 (green) showing loss actin staining (red) of proximal tubular brush border (arrowhead) and epithelial breakdown (arrow). Scale bar = 30 μm .

Table S1. Primers used for qRT-PCR.

This material is available as part of the online article from:

<http://www.blackwell-synergy.com/doi/abs/10.1111/j.1462-5822.2008.01182.x>

Please note: Blackwell Publishing is not responsible for the content or functionality of any supplementary materials supplied by the authors. Any queries (other than missing material) should be directed to the corresponding author for the article.